Journal of Crystal Growth 588 (2022) 126654

Contents lists available at ScienceDirect

Journal of Crystal Growth

journal homepage: www.elsevier.com/locate/jcrysgro

Effects of InGaN quantum disk thickness on the optical properties of GaN nanowires

Syed M N Hasan [a], Arnob Ghosh [a], Sharif Md Sadaf [b,*], Shamsul Arafin [a,*]

[a] Department of Electrical and Computer Engineering, The Ohio State University, Columbus, OH 43210, USA
[b] Institut National De La Recherche Scientifique (INRS), Varennes, QC, Canada

ARTICLE INFO

Keywords:
A1. Characterization
A1. Nanostructures
A3. Molecular beam epitaxy
B1. Nanomaterials
B1. Nitrides
B2. Semiconducting indium compounds

ABSTRACT

The impact of InGaN quantum disk (Qdisk) thickness on the optical emission properties of axial InGaN/GaN nanowires is experimentally studied. The luminescence of InGaN/GaN nanowire heterostructures grown by plasma assisted molecular beam epitaxy were measured using a combination of photoluminescence and cathodoluminescence spectroscopy. The variation of peak emission wavelength, spectral lineshape, width, and maximum intensity with the change of Qdisk thickness over the range of 4–12 nm was systematically analyzed. Both the spectroscopic measurements from the average InGaN Qdisk-related emissions reveal the presence of built-in piezoelectric strain as evidenced by the luminescence blueshift with increasing pump signal. To determine the material compositions and their spatial uniformity across the stacked InGaN Qdisks separated by GaN barriers, transmission electron microscopy with energy-dispersive x-ray spectroscopy were also performed. This provides further insights into the structural properties of the InGaN Qdisks within GaN nanowires. Thus, our experimental study serves to advance the understanding of, in general, III-nitride nanostructures for the implementation of classical and non-classical optoelectronic devices.

1. Introduction

One-dimensional (1D) compound semiconductor nanostructures have recently attracted remarkable research attention due to their great promise to implement high-performance “quantum” devices such as single photon emitters (SPEs) [1] and single photon detectors [2] in addition to their decades-long use in realizing “classical” elements including light emitting diodes [3], lasers [4], photodetectors [5] and solar cells [6]. Owing to their unique electronic and optical properties arising from the anisotropic geometry, large surface-to-volume ratios, and excellent carrier and photon confinement in two dimensions, such nanostructures have been exploited to demonstrate novel functional optoelectronic devices for the last decade. Moreover, 1D structures allow to produce crystalline materials with a low defect density on a variety of foreign substrates, including metals and silicon [3,7,8].

Among the material platforms, III-nitride heterostructures have gained significant prominence and shown great potential in realizing tunable light emitting devices in a broad spectral region because of the tremendous progress in *p*-doped GaN and InGaN/GaN active region [1,9,10]. In particular, InGaN/GaN NW heterostructures have shown tremendous promise for applications in solid-state lighting. To achieve more scientific and technological breakthroughs in optoelectronic device applications beyond solid-state lighting, further intellectual understanding, and improved knowledge in optical emission properties of InGaN/GaN NW heterostructures are of utmost importance. InGaN quantum dots (QDs) [1,11] or quantum disks (Qdisks) [12]-in-a-wire are the two popular nanostructures which have been extensively studied and successfully used for fabricating high-performance light emitters at the blue and green spectral regimes and phosphor-free white LEDs. The optical narrow/broadband emission in these studies [11,13] was engineered by varying the In compositions and/or the size of the dots or disks. InGaN dot/disk-in-a wire nanostructures have also been employed to demonstrate the novel tunable SPEs [14–17].

Although high In incorporation in dots/disks of these NWs is proven to be technically challenging, changing the QD or Qdisk geometry, e.g., thickness, is relatively easier to tailor the optical emission. However, the InGaN QDor Qdisk thickness in these NWs is usually limited to only 3-4 nm [18,19] for the reduction of quantum confined Stark effect (QCSE). Considering the fact that thicker QWs are expected to offer a higher radiative recombination rate, leading to a large material gain to result in high emission intensity and leveraging the NW environment to attain less strain, this experimental study investigates the impact of Qdisk

* Corresponding authors.
E-mail addresses: najibhasan.1@osu.edu (S. M N Hasan), ghosh.230@osu.edu (A. Ghosh), sharif.sadaf@inrs.ca (S. Md Sadaf), arafin.1@osu.edu (S. Arafin).

https://doi.org/10.1016/j.jcrysgro.2022.126654
Received 7 January 2022; Received in revised form 16 March 2022; Accepted 31 March 2022
Available online 1 April 2022

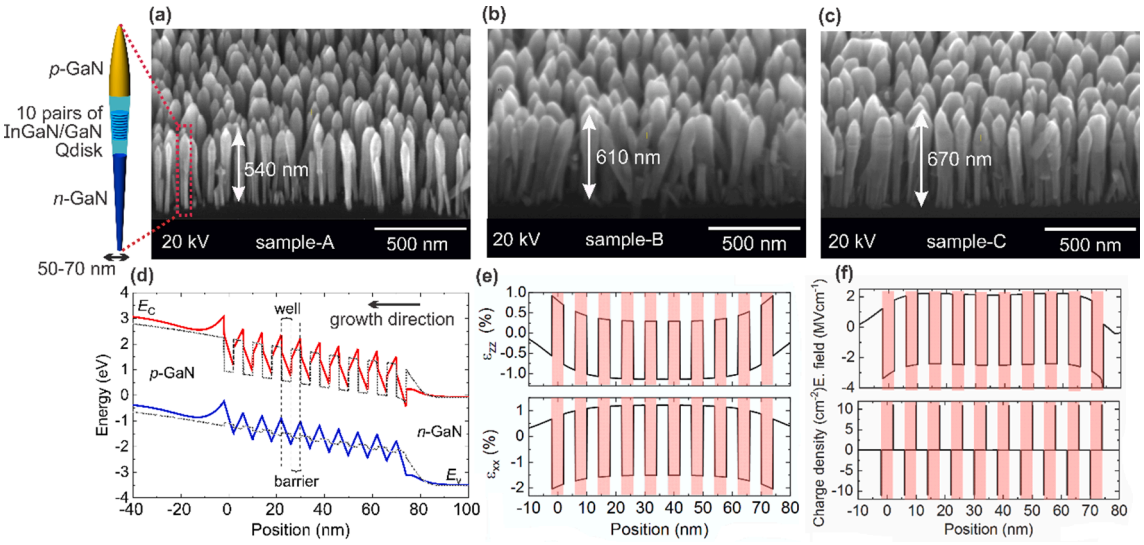

Fig. 1. (a)–(c) 45°-titled SEM images of the three InGaN/GaN NW control samples with different Qdisk thickness, schematic view of a representative NW of the samples is also shown at the left, (d) simulated band diagram with and without polarization, (e) strain distribution and (f) polarization field and sheet charge density within the Qdisks.

thickness on emission intensity, and peak emission wavelength of InGaN/GaN NWs. Our results correlate with the previous counterintuitive findings on the influence of strain on the InGaN/GaN NWs [20,21].

In this work, the optical emission characteristics of the InGaN Qdisks embedded in GaN NWs were determined using photoluminescence (PL), and cathodoluminescence (CL) spectroscopy at room-temperature. Morphological and structural characteristics of the NWs were studied by scanning electron microscopy (SEM) and transmission electron microscopy (TEM), respectively. In compositional fluctuations, and QCSE present in the stacked InGaN/GaN Qdisks were also explored. A systematic analysis of the emission energy and intensity coming from the NW samples makes it possible to observe correlations between Qdisk geometry, emission energy shift, and emission rates. The results suggest that the emission wavelength and intensity from the NWs are dependent on the Qdisk thickness. Thicker InGaN Qdisks are also expected to reduce the defects present at the InGaN/GaN interfaces and result in an improved radiative recombination rate.

2. Experimental description

The *p-i-n* NW structures were grown catalyst-free on *n*-type silicon (1 1 1) substrates using plasma-assisted molecular beam epitaxy (PAMBE) under N_2-rich conditions. The growth of *n*-GaN nanowires was initiated by depositing a few monolayers of gallium (Ga) for 6 sec before the nitrogen plasma struck. Following the growth of ~200 nm of Si-doped GaN layer at 775 °C, the growth temperature was reduced to 650 °C to grow InGaN/GaN active regions. Throughout the growth, N_2 flow was fixed at 2.5 sccm with a radio-frequency power of 300 W. During the active region growth, the Ga and In sources beam equivalent pressures (BEPs) were set to 3.5×10^{-8} and 4.7×10^{-8} Torr, respectively, while for both *n*- and *p*-GaN, the Ga BEP was set to 5.4×10^{-8} Torr. After the deposition of Qdisk-based active region, we adjusted the growth temperature to only 755 °C to minimize the thermal desorption of the InGaN Qdisks and proceeded with the growth of 150-nm-thick Mg-doped GaN layer. Three different control samples, each with 10 pairs of InGaN Qdisks/GaN barriers with varying Qdisk thicknesses, were grown in our study. While keeping GaN barrier thickness constant at ~5 nm for the three samples, InGaN Qdisk thickness was increased from 4 nm in sample-A, to 9 nm of sample-B, and 12 nm of sample-C.

The optical properties of each sample were studied using room-temperature PL spectroscopy. For the PL measurement, a continuous-wave 405 nm laser with a variable excitation power and a spot diameter of ~3 mm was used. A Zeiss Ultra Plus standard detector SEM system at an accelerating voltage of 20 kV was used to determine the morphology of the three NW samples. The CL imaging and spectra were measured by a Horiba H-Clue CL system with an iHR320 spectrometer and Synapse CCD with sensitivity from 200 nm to 900 nm integrated with a Thermo Scientific Quattro environmental scanning electron microscope (ESEM). The accelerating voltage for CL observation was 10 kV for optimal CL intensity and spatial resolution. The chemical compositions of the NWs were investigated by high-angle annular dark-field scanning transmission electron-microscopy (HAADF-STEM) on a JEOL 3100R05 double-corrected STEM operated at 300 kV with energy-dispersive x-ray spectroscopy (EDS).

3. Results and discussions

Fig. 1(a), (b) and (c) show the 45° tilted view of the three Qdisks-in-NWs samples under study. The spontaneously grown NWs develops an inverse-tapered shape both on the top and bottom, as schematically shown in top-left of Fig. 1. It is also seen that the average diameter from sample-A to -C increases as the NW height increases. The growth of *p*-GaN grown on top of the active region creates a shell-like structure around the NW since Mg promotes lateral growth [22]. Formation of boundary dislocations and increase of average tilting results by coalescence of misoriented NWs, resulting in poor structural and optical properties [23,24]. As can be seen, nanowire coalescences were completely avoided for all the three samples.

To get a better insight about the degree of strain on Qdisks and its effects on conduction and valance bands, strain minimization calculations were done based on the continuum elasticity model and self-consistent Schrödinger-Poisson equation. 3D numerical simulations were performed to calculate the band diagram that considered 10 pairs of InGaN Qdisks and GaN barriers each having 4 nm thickness and 50 nm diameter (Fig. 1(d)). The dotted line represents the band diagram without considering the polarization effect, i.e. no QCSE (Fig. 1(d)). The in-plane (ε_{xx}) and c-plane (ε_{zz}) strain tensors along the Qdisk center were calculated and shown in Fig. 1(e). It was found that along the in-plane axis Qdisks represented by the shaded regions are compressively (−1.5 ~ −2%) strained, and along c-axis the Qdsiks experience lattice expansion (0.3 ~ 0.9%). Due to this strain along the c-axis, piezoelectric polarization induced sheet charges in the InGaN/GaN interfaces

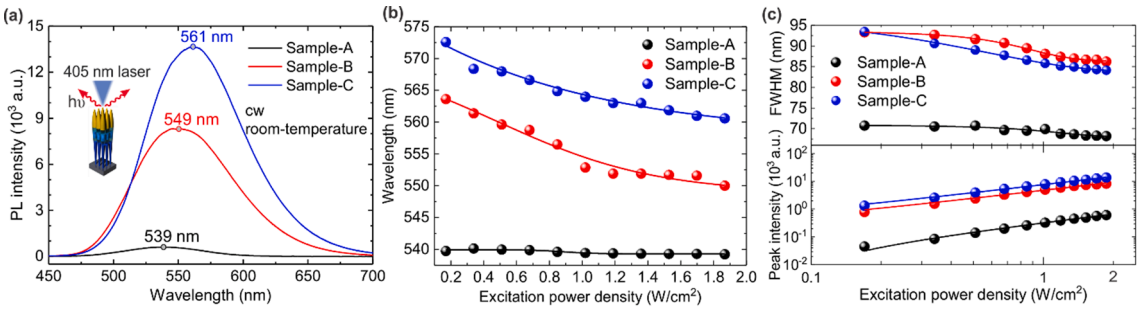

Fig. 2. (a) Unnormalized PL spectra at a fixed excitation power, excitation power dependent measurement for (b) emission wavelength, and (c) full width at half maximum (top) and peak PL intensity (bottom) of the three InGaN/GaN NW control samples.

correspond to an internal electric field of as high as 2.1 MVcm^{-1}, which is shown in Fig. 1(f). This internal electric field is responsible for a shift of the ground-level transition energy ΔE, leading to a change in the PL and CL emission wavelengths. This is evident in the following analytic expression based on the perturbation theory [25],

$$\Delta E = -\frac{512(m_e + m_h)e^2F^2d^4}{243\pi^6\hbar^2\chi^2}$$

where e is the elementary charge, F the internal field strength, d the disk width and m_e and m_h electron and hole carrier masses, respectively. Here χ represents the screening of the internal electric field by the carriers in the Qdisk as given by $\chi = 1 + \frac{n}{n_{scr}}$ where,

$$n_{scr} = \frac{27\pi^3\varepsilon_r\varepsilon_0\hbar^2}{80e^2d^3(m_e + m_h)}$$

is a screening coefficient, ε_0 and ε_r the vacuum permittivity and the relative permittivity of the disk material, respectively. Hence, the screening of the QCSE is strongly dependent on the concentration of the electron–hole pairs which increase with increasing excitation power density in our PL and CL measurements. This, in turn, reduces the shift of the ground-level transition energy, resulting in a blue shift of the emission wavelength.

Fig. 2(a) presents the unnormalized room temperature-PL spectra of the three control samples, showing the emission wavelengths shift to longer wavelengths with increasing Qdisk thickness. The measured peak emission wavelengths of sample-A, -B and -C are 539 nm, 549, nm and 561 nm, respectively. This could be explained by the InGaN/GaN mismatch-induced piezoelectric polarization field and the resulting increased QCSE with the increase of InGaN Qdisk thickness [26–28]. Another well-known phenomenon observed in InGaN is random alloy fluctuations. With the increase of the total active area volume, randomly distributed In-rich clusters also increase, leading to a high localization potential even at room temperature. The thicker Qdisks create a deeper localization potential which contributes to the redshift in the emission spectra as well [29].

To interpret the effects of Qdisk thickness, PL spectra were acquired as a function of excitation power at room temperature, as shown in Fig. 2

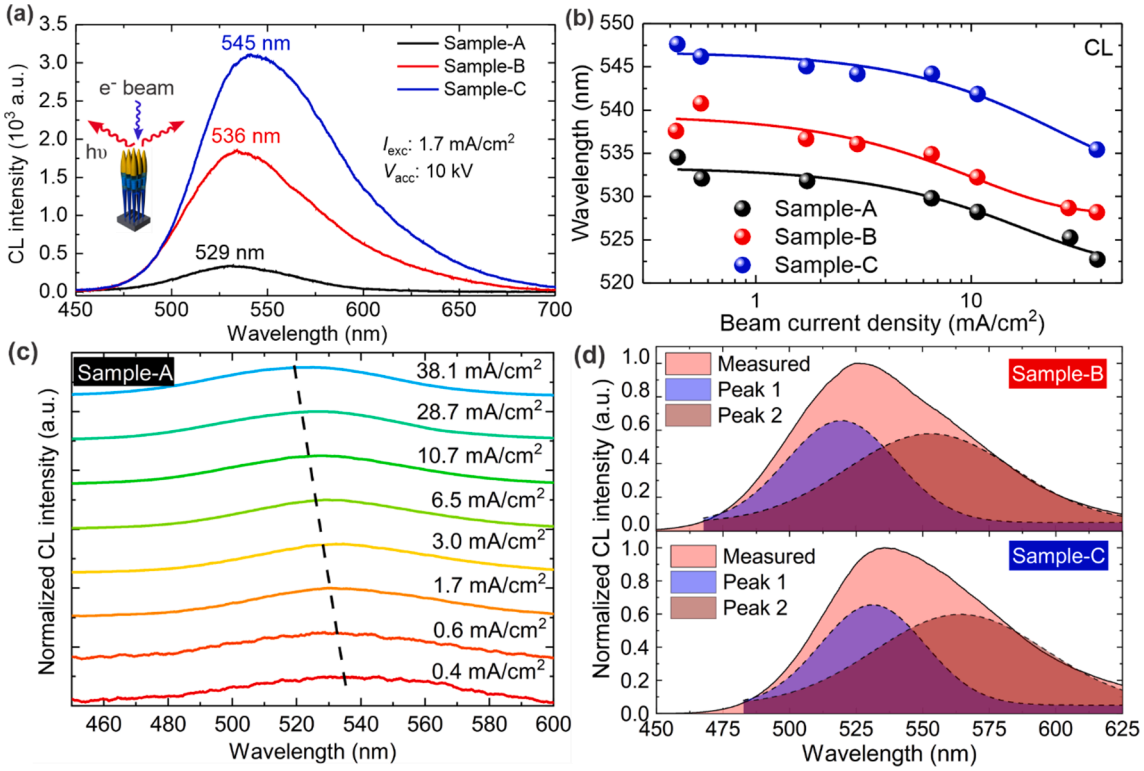

Fig. 3. (a) Room-temperature unnormalized CL spectra of the three control samples, (b) peak wavelengths shift as a function of excitation current density of the three control samples, (c) excitation current dependent CL spectra for sample-A, and (d) bimodal In compositional distribution of CL spectra for sample-B and sample-C along with bi-Gaussian fitted peaks, the shorter peak wavelength as peak-1 and the longer peak wavelength as peak-2.

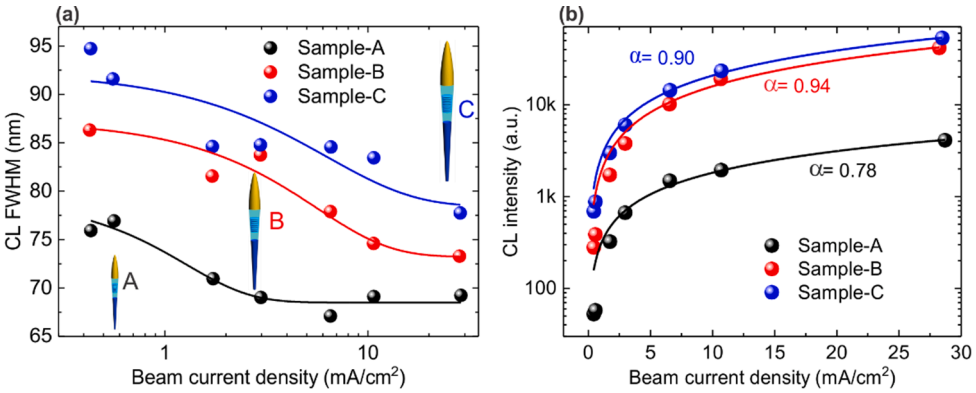

Fig. 4. (a) The change of CL FWHM, and (b) CL intensity as a function of beam current density; the solid line in (b) represents the power law fit to the measured data points.

(b). As excitation power increases, the PL peaks of both sample-B and -C exhibit a blueshift by approximately 13 nm, while the sample-A shows almost no change with the excitation power. This blueshift could be attributed to three possible mechanisms including piezoelectric field-induced QCSE compensated by a free-carrier screening effect, band-filling effect and localized carrier potential. The band titling due to QCSE results in a redshift and is a function of the InGaN thickness. Increasing the laser excitation powers weakens the QCSE and increases transition energy resulting in a blueshift [30]. Thus, no blueshift was observed for sample-A due to a very small built-in piezoelectric field at the Qdisk-based active region unlike the other two thicker InGaN Qdisk samples. While the band-filling effect with increasing excitation power may also cause the blueshift in the emission wavelengths [31,32], this leads to broadening of the PL linewidth, i.e. larger FWHM [33,34]. The third mechanism, localization of carrier potential is directly related to both In-fluctuation in the Qdisks, and internal electric field and thus promoted by larger Qdisk thickness, which also results in higher PL linewidth [35,36]. Interestingly, linewidth narrowing is observed with increasing excitation power as shown in Fig. 2(c), indicating that QCSE compensation is the most probable mechanism of the PL blueshift. Fig. 2 (c) also presents the PL peak intensity for each sample under different excitation powers. The larger active region volume of the thicker Qdisk samples results in carrier distribution along the Qdisk stack, which ensures a low carrier density compared to the thin Qdisks [37]. The lower carrier density ensures suppression of non-radiative Auger recombination and efficient radiative transition. Due to the increase in the radiative recombination rates, sample-B and -C are found to be nearly 20× and 30× brighter compared to sample-A. The PL intensity increases linearly with excitation power with no apparent intensity saturation. The ~1 value of the slope for all the three control samples indicate that the band-to-band radiative recombination process is dominant which could be due to carrier localization effect, as it is widely accepted that at room temperature carrier localization plays a significant role in overcoming non-radiative recombination paths.

To further investigate the optical emission properties, the control samples were further analyzed using the CL system with a much higher spatial resolution and sensitivity. A redshift in peak emission wavelength similar to the PL spectra is observed in the RT-CL spectra with increasing the Qdisk thickness, as shown in Fig. 3(a). The CL peak wavelengths as a function of excitation current densities of all the samples is presented in Fig. 3(b). Interestingly, the beam current dependent CL spectra for each sample show slightly different emission characteristics from the excitation power dependent PL. Like the PL data, the blueshift in the peak CL emission wavelengths with increasing beam current is observed for the control samples except sample-A.

Since QCSE increases with increasing the Qdisk thickness, a larger blueshift of emission wavelengths was intuitively expected in sample-B and -C with thicker Qdisks. Interestingly, the total blueshift with the change of beam current is measured to be nearly same among the three control samples. Moreover, the total CL blueshift in the entire beam current range is lower than the PL blueshifts for each respective sample, presumably due to larger carrier screening effect in CL measurements. Beside the blueshift, another notable difference between the CL and PL emission was observed in sample-A. The small beam spot size and high spatial resolution of the CL system was leveraged for sample-A with low optical emission. The low optical emission as well as large-area excitation in PL did not give a true representation of our Qdisk-in-NW structures with no piezoelectric strain. With a small beam spot size of 2 μm × 2 μm, the impact of random size distribution among spontaneously-formed NWs and In compositional fluctuations on CL spectra can be somewhat minimized. The near identical blueshift for samples with different InGaN thickness indicates that the QCSE induced redshift of the emission wavelength is not changing with the increase of InGaN thickness and could be determined by the InGaN/GaN interfaces [38] which were fixed for all the three samples.

Fig. 3(c) shows the excitation beam current dependent CL spectra obtained for various beam current density for Sample--A. While the energy band tilting remained the same, the emission spectra changed as the Qdisk thickness increases. For Sample-A, the spectra were fitted with Gaussian functions, while the other two samples show asymmetric spectra which were deconvoluted to two individual component spectra with the overlapping emissions. Fig. 3(d) shows the CL emission spectra for samples -B and -C where a bimodal distribution of In compositions is seen. The presence of the bimodal distribution can be related to the In compositional fluctuations present in the InGaN Qdisks [39]. Due to quantum size effects, a redshift of the deconvoluted peaks is recorded as the Qdisk thickness increases from sample-B to sample-C.

The superior optical characteristics in terms of the minimal blueshift with higher excitation current and higher emission intensity for sample-B and -C is further related to the reduction of point defects, dislocations while growing a thicker layer without interfaces too close to each other. The similar behavior was also observed in thin film structures where a single, thicker quantum well structure resulted in a higher internal quantum efficiency and significantly longer carrier lifetime compared to a multi-quantum well (QW) structure with equal volume and same material [40]. Reduction of interface defects such as Ga vacancies and alloy fluctuation by growing thicker QWs were responsible for the improved carrier lifetime [41,42]. The difference between the thinnest Qdisk sample (sample-A) and the other two thus can be seen as a result of reduced interaction between the interfaces due to thicker Qdisks and improved radiative recombination rate with a limited wave function separation. However, emission intensity as a function of excitation current shown in Fig. 4(b) revealed near identical intensity for sample-B and -C. This indicates that optical performance improvement with thicker Qdisk reaches to a saturation point. The CL intensities were then further fitted using the power law, $I \sim P^{\alpha}$, to evaluate the recombination

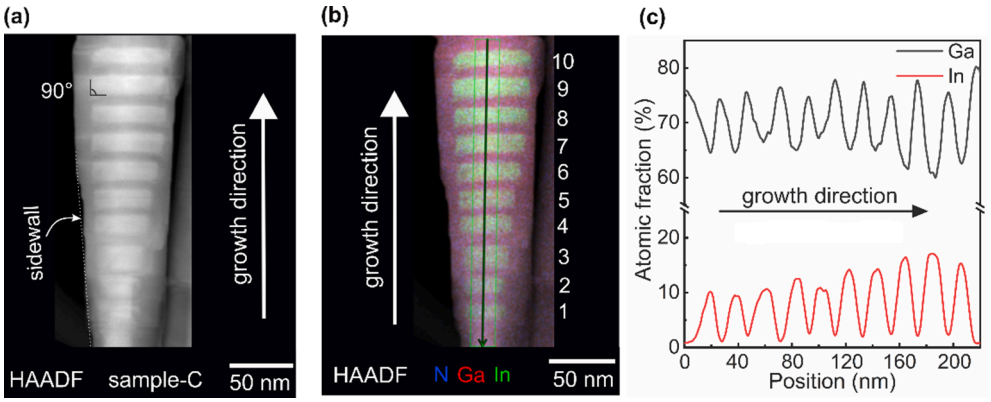

Fig. 5. (a) HAADF-STEM image, (b) the corresponding EDS mapping and (c) the atomic elemental profile of sample-C. The growth directions are indicated by the arrows.

mechanisms involved in CL spectra of the InGaN Qdisk. Here, I is the emission intensity, P the excitation power, and α a fitting parameter to represent various recombination processes [43,44]. The value of α for each sample is mentioned next to the fitted lines. The non-linear dependence observed with $\alpha < 1$ values indicate the existence of "free-to-bound" and "donor-acceptor pair" recombination processes while $\alpha = 1$ indicates the radiative recombination process dominates. The origin of $\alpha < 1$ values often can be related to the In or Ga vacancies acting as acceptors and N-related donor point defects [45,46]. For sample-A, $\alpha = 0.78$ indicates the existence of these sites due to the interface fluctuation in the thinner wells whereas for B and C, the similar values are obtained to be 0.94 and 0.9, respectively, yielding superior material quality. A near saturation point at a current density > 20 mA/cm^2 results from the filled density of states associated with the defects. Although photon quenching was previously reported in InGaN QWs [47], the $\alpha < 1$ values of the curves for our three samples is not likely to be caused by this phenomenon. This is not only because of the use of NW materials with reduced defects and deep level traps but also our CL measurements were conducted at a low-injection level (<50 mA/cm^2) where Auger process and photon quenching are less likely to be triggered.

Fig. 5 (a)-(b) shows the HAADF-STEM and EDS images for sample-C, showing the 10 stacks of InGaN Qdisks are interfaced with GaN barriers. As could be expected, the only geometric change in the TEM data of sample-A and -B with respect to sample-C is the Qdisk thickness. A progressive increase of the Qdisk width can be seen along the growth direction. The 90° angle between the c-plane and side-facets indicates a strain free InGaN/GaN interface which is maintained throughout the InGaN/GaN pairs. The atomic elemental mapping data for 10 InGaN Qdisks is shown in Fig. 5(c). A low In-content at the first couple of Qdisks indicates that In-incorporation is hindered at the initial stages of the growth and gradually reaches to a desired value. This progressive increase of In-content can be attributed to the compositional pulling effect [21,48]. A slight reduction in the growth temperature after the deposition of a few QDs also improves the In sticking coefficient. This yields a relatively high In-content with less compositional fluctuations along the growth direction. The tapered sidewall morphology at the NW center of sample-C is due to the low growth temperature at the NW top that promotes lateral growth with a reduced adatom diffusion length.

4. Summary

In conclusion, a detailed investigation on the optical and structural properties of InGaN/GaN Qdisk-in-NW heterostructures was experimentally conducted. It is found that the emission intensity and peak wavelength of the NWs strongly depend on the Qdisk thickness, suggesting that optical emission can be tailored even without changing In compositions. The change in optical properties was explained using the PL and CL spectral data. The excitation power dependent luminescence measurements also relate with both compositional fluctuation and QCSE which are claimed to be the principal reasons of the blueshift of the peak wavelength. While most of the strain is expected to be screened out of the material near the Si-GaN interface, the presence of a certain degree of elastic strain was evident for the NWs, which eventually creates a bimodal In compositional distribution in the thicker InGaN Qdisks. Despite the bimodality, our study encourages using thicker InGaN/GaN active regions to simultaneously enable high quantum efficiency and tune emission wavelengths.

CRediT authorship contribution statement

Syed M N Hasan: Material Growth, Characterization, Writing – original draft. **Arnob Ghosh:** Material Characterization, Theoretical Analysis. **Sharif Md Sadaf:** Conceptualization, Supervision. **Shamsul Arafin:** Conceptualization, Writing – review & editing.

Declaration of Competing Interest

The authors declare that they have no known competing financial interests or personal relationships that could have appeared to influence the work reported in this paper.

Acknowledgement

This research was funded by the National Science Foundation (NSF) under grant number 2020015. Electron microscopy was performed at the Center for Electron Microscopy and Analysis (CEMAS) at The Ohio State University.

References

[1] S. Deshpande, J. Heo, A. Das, P. Bhattacharya, Electrically driven polarized single-photon emission from an InGaN quantum dot in a GaN nanowire, Nat. Commun. 4 (1) (2013) 1.
[2] D. Leopold, J. Buckley, P. Rebillot, High quantum efficiency ultraviolet/blue AlGaN/ InGaN photocathodes grown by molecular-beam epitaxy, J. Appl. Phys. 98 (4) (2005) 043525.
[3] W. Guo, M. Zhang, A. Banerjee, P. Bhattacharya, Catalyst-free InGaN/GaN nanowire light emitting diodes grown on (001) silicon by molecular beam epitaxy, Nano Lett. 10 (9) (2010) 33559.
[4] S. Arafin, X. Liu, Z. Mi, Review of recent progress of III-nitride nanowire lasers, J. Nanophotonics 7 (1) (2013) 074599.
[5] A. Aiello, A.K.M.H. Hoque, M.Z. Baten, P. Bhattacharya, High-gain silicon-based InGaN/GaN dot-in-nanowire array photodetector, ACS Photonics 6 (5) (2019) 1289–1294.
[6] R. Cheriton, S. Sadaf, L. Robichaud, J. Krich, Z. Mi, K. Hinzer, Two-photon photocurrent in InGaN/GaN nanowire intermediate band solar cells, Commun. Mater. 1 (1) (2020) 1.

[7] S.M. Sadaf, Y.-H. Ra, S. Zhao, T. Szkopek, Z. Mi, Structural and electrical characterization of monolithic core–double shell *n*-GaN/Al/*p*-AlGaN nanowire heterostructures grown by molecular beam epitaxy, Nanoscale 11 (9) (2019) 3888–3895.

[8] S.M. Sadaf, Y.H. Ra, T. Szkopek, Z. Mi, Monolithically integrated metal/semiconductor tunnel junction nanowire light-emitting diodes, Nano Lett. 16 (2) (2016) 1076–1080.

[9] T. Kuykendall, P. Ulrich, S. Aloni, P. Yang, Complete composition tunability of InGaN nanowires using a combinatorial approach, Nat. Mater. 6 (12) (2007) 951–956.

[10] S. Sadaf, H. Tang, Mapping the growth of *p*-type GaN layer under Ga-rich and N-rich conditions at low to high temperatures by plasma-assisted molecular beam epitaxy, Appl. Phys. Lett. 117 (25) (2020) 254104.

[11] H.P.T. Nguyen, S. Zhang, A.T. Connie, M.G. Kibria, Q.i. Wang, I. Shih, Z. Mi, Breaking the carrier injection bottleneck of phosphor-free nanowire white light-emitting diodes, Nano Lett. 13 (11) (2013) 5437–5442.

[12] R. Bardoux, A. Kaneta, M. Funato, Y. Kawakami, A. Kikuchi, K. Kishino, Positive binding energy of a biexciton confined in a localization center formed in a single $In_xGa_{1-x}N$/GaN quantum disk, Phys. Rev. B 79 (15) (2009) 155307.

[13] X. Sun, P. Wang, T. Wang, L. Chen, Z. Chen, K. Gao, T. Aoki, M. Li, J. Zhang, T. Schulz, M. Albrecht, W. Ge, Y. Arakawa, B. Shen, M. Holmes, X. Wang, Single-photon emission from isolated monolayer islands of InGaN, Light Sci. Appl. 9 (1) (2020) 1.

[14] M.J. Holmes, K. Choi, S. Kako, M. Arita, Y. Arakawa, Room-temperature triggered single photon emission from a III-nitride site-controlled nanowire quantum dot, Nano Lett. 14 (2) (2014) 982–986.

[15] E. Chernysheva, Ž. Gačević, N. García-Lepetit, H. Meulen, M. Müller, F. Bertram, P. Veit, A. Torres-Pardo, J. Calbet, J. Christen, E. Calleja, Blue-to-green single photons from InGaN/GaN dot-in-a-nanowire ordered arrays, EPL (Europhys. Lett.) 111 (2) (2015) 24001.

[16] T.J. Puchtler, T. Wang, C.X. Ren, F. Tang, R.A. Oliver, R.A. Taylor, T. Zhu, Ultrafast, polarized, single-photon emission from m-plane InGaN quantum dots on GaN nanowires, Nano Lett. 16 (12) (2016) 7779–7785.

[17] P. Michler, Quantum dots for quantum information technologies, Springer, 2017.

[18] L. Redaelli, A. Mukhtarova, S. Valdueza-Felip, A. Ajay, C. Bougerol, C. Himwas, J. Faure-Vincent, C. Durand, J. Eymery, E. Monroy, Effect of the quantum well thickness on the performance of InGaN photovoltaic cells, Appl. Phys. Lett. 105 (13) (2014) 131105.

[19] R. Wang, H. Nguyen, A. Connie, J. Lee, I. Shih, Z. Mi, Color-tunable, phosphor-free InGaN nanowire light-emitting diode arrays monolithically integrated on silicon, Opt. Express 22 (107) (2014) A1768.

[20] G. Tourbot, C. Bougerol, F. Glas, L. Zagonel, Z. Mahfoud, S. Meuret, P. Gilet, M. Kociak, B. Gayral, and B. Daudin, "Growth mechanism and properties of InGaN insertions in GaN nanowires," *Nanotechnology,* vol. 23, no. 13, p. 135703, 2012.

[21] G. Tourbot, C. Bougerol, A. Grenier, M. Den Hertog, D. Sam-Giao, D. Cooper, P. Gilet, B. Gayral, B. Daudin, Structural and optical properties of InGaN/GaN nanowire heterostructures grown by PA-MBE, Nanotechnology 22 (7) (2011) 075601.

[22] F. Furtmayr, M. Vielemeyer, M. Stutzmann, J. Arbiol, S. Estradé, F. Peirò, J. Morante, M. Eickhoff, Nucleation and growth of GaN nanorods on Si (111) surfaces by plasma-assisted molecular beam epitaxy-The influence of Si-and Mg-doping, J. Appl. Phys. 104 (3) (2008) 034309.

[23] G. Calabrese, D. van Treeck, V.M. Kaganer, O. Konovalov, P. Corfdir, C. Sinito, L. Geelhaar, O. Brandt, S. Fernández-Garrido, Radius-dependent homogeneous strain in uncoalesced GaN nanowires, Acta Mater. 195 (2020) 87–97.

[24] V. Consonni, M. Knelangen, U. Jahn, A. Trampert, L. Geelhaar, H. Riechert, Effects of nanowire coalescence on their structural and optical properties on a local scale, Appl. Phys. Lett. 95 (24) (2009) 241910.

[25] K.A. Bulashevich, S.Y. Karpov, R.A. Suris, Analytical model for the quantum-confined Stark effect including electric field screening by non-equilibrium carriers, *Phys. Status Solidi (B)* 243 (7) (2006) 1625–1629.

[26] S.F. Chichibu, A.C. Abare, M.S. Minsky, S. Keller, S.B. Fleischer, J.E. Bowers, E. Hu, U.K. Mishra, L.A. Coldren, S.P. DenBaars, T. Sota, Effective band gap inhomogeneity and piezoelectric field in InGaN/GaN multiquantum well structures, Appl. Phys. Lett. 73 (14) (1998) 2006–2008.

[27] T. Takeuchi, S. Sota, M. Katsuragawa, M. Komori, H. Takeuchi, H. Amano, I. Akasaki, Quantum-confined Stark effect due to piezoelectric fields in GaInN strained quantum wells, Jpn. J. Appl. Phys. 36 (4A) (1997) L382.

[28] D. Koleske, A. Fischer, B. Bryant, P. Kotula, and J. Wierer, "Underlying Mechanisms of Increased Efficiency in InGaN-Based Multiple Quantum Wells Emitting at 530-590 nm with AlGaN Interlayers," Sandia National Lab.(SNL-NM), Albuquerque, NM (United States), 2014.

[29] J. Bai, T. Wang, S. Sakai, Influence of the quantum-well thickness on the radiative recombination of InGaN/GaN quantum well structures, J. Appl. Phys. 88 (8) (2000) 4729.

[30] K. Lai, T. Paskova, V. Wheeler, J. Grenko, M. Johnson, D. Barlage, K. Udwary, E. Preble, K. Evans, Excitation current dependent cathodoluminescence study of InGaN/GaN quantum wells grown on m-plane and c-plane GaN substrates, J. Appl. Phys. 106 (11) (2009) 113104.

[31] H. Murotani, H. Andoh, T. Tsukamoto, T. Sugiura, Y. Yamada, T. Tabata, Y. Honda, M. Yamaguchi, H. Amano, Emission Wavelength Dependence of Internal Quantum Efficiency in InGaN Nanowires, Jpn. J. Appl. Phys. 52 (8S) (2013) pp. 08JE10.

[32] H. Murotani, Y. Yamada, T. Tabata, Y. Honda, M. Yamaguchi, H. Amano, Effects of exciton localization on internal quantum efficiency of InGaN nanowires, J. Appl. Phys. 114 (15) (2013) 153506.

[33] E. Kuokstis, J.W. Yang, G. Simin, M.A. Khan, R. Gaska, M.S. Shur, Two mechanisms of blueshift of edge emission in InGaN-based epilayers and multiple quantum wells, Appl. Phys. Lett. 80 (6) (2002) 977–979.

[34] T. Stoica, R.J. Meijers, R. Calarco, T. Richter, E. Sutter, H. Lüth, Photoluminescence and intrinsic properties of MBE-grown InN nanowires, Nano Lett. 6 (7) (2006) 1541–1547.

[35] G. Weng, W. Zhao, S. Chen, H. Akiyama, Z. Li, J. Liu, B. Zhang, Strong localization effect and carrier relaxation dynamics in self-assembled InGaN quantum dots emitting in the green, Nanoscale Res. Lett. 10 (1) (2015) 1.

[36] Y. Yoo, J. Na, S. Son, Y. Cho, Effective suppression of efficiency droop in GaN-based light-emitting diodes: role of significant reduction of carrier density and built-in field, Sci. Rep. 6 (1) (2016) 1.

[37] G. Muziol, H. Turski, M. Siekacz, K. Szkudlarek, L. Janicki, S. Zolud, R. Kudrawiec, T. Suski, and C. Skierbiszewski, "Highly efficient optical transition between excited states in wide InGaN quantum wells," *arXiv preprint arXiv:1810.07612,* 2018.

[38] M. Tangi, P. Mishra, B. Janjua, A. Prabaswara, C. Zhao, D. Priante, J. Min, T. Ng, B. Ooi, Role of quantum-confined stark effect on bias dependent photoluminescence of N-polar GaN/InGaN multi-quantum disk amber light emitting diodes, J. Appl. Phys. 123 (10) (2018) 105702.

[39] S. Woo, N. Gauquelin, H. Nguyen, Z. Mi, G. Botton, Interplay of strain and indium incorporation in InGaN/GaN dot-in-a-wire nanostructures by scanning transmission electron microscopy, Nanotechnology 26 (34) (2015) 344002.

[40] S. Okur, M. Nami, A. Rishinaramangalam, S. Oh, S. DenBaars, S. Liu, I. Brener, D. Feezell, Internal quantum efficiency and carrier dynamics in semipolar (2021) InGaN/GaN light-emitting diodes, Opt. Express 25 (3) (2017) 2178.

[41] S. Marcinkevičius, K. Kelchner, L. Kuritzky, S. Nakamura, S. DenBaars, J. Speck, Photoexcited carrier recombination in wide m-plane InGaN/GaN quantum wells, Appl. Phys. Lett. 103 (11) (2013) 111107.

[42] G.A. Garrett, H. Shen, M. Wraback, A. Tyagi, M.C. Schmidt, J.S. Speck, S. P. DenBaars, S. Nakamaura, Comparison of time-resolved photoluminescence from InGaN single quantum wells grown on nonpolar and semipolar bulk GaN substrates, Phys. Status Solidi C 6 (S2) (2009) S800–S803.

[43] T. Schmidt, K. Lischka, W. Zulehner, Excitation-power dependence of the near-band-edge photoluminescence of semiconductors, Phys. Rev. B 45 (16) (1992) 8989–8994.

[44] M. Tangi, J.-W. Min, D. Priante, R.C. Subedi, D.H. Anjum, A. Prabaswara, N. Alfaraj, J.W. Liang, M.K. Shakfa, T.K. Ng, B.S. Ooi, Observation of piezotronic and piezo-phototronic effects in n-InGaN nanowires/Ti grown by molecular beam epitaxy, Nano Energy 54 (2018) 264–271.

[45] F. Reurings, F. Tuomisto, C.S. Gallinat, G. Koblmüller, J.S. Speck, In vacancies in InN grown by plasma-assisted molecular beam epitaxy, Appl. Phys. Lett. 97 (25) (2010) 251907.

[46] M. Tangi, A. De, S. Shivaprasad, Role of dislocations and carrier concentration in limiting the electron mobility of InN films grown by plasma assisted molecular beam epitaxy, J. Appl. Phys. 123 (1) (2018) 015701.

[47] R. Sarkissian, S. Roberts, T. Yeh, S. Das, S. Bradforth, J. O'Brien, P. Dapkus, Photon quenching in InGaN quantum well light emitting devices, Appl. Phys. Lett. 103 (4) (2013) 041123.

[48] Y. Kawaguchi, M. Shimizu, M. Yamaguchi, K. Hiramatsu, N. Sawaki, W. Taki, H. Tsuda, N. Kuwano, K. Oki, T. Zheleva, R.F. Davis, The formation of crystalline defects and crystal growth mechanism in $In_xGa_{1-x}N$/GaN heterostructure grown by metalorganic vapor phase epitaxy, J. Cryst. Growth 189-190 (1998) 24–28.